EUROPEAN FUSION DEVELOPMENT AGREEMENT

EFDA–JET–PR(05)11

E. Asp, J. Weiland, X. Garbet, V. Parail, P. Strand and JET EFDA contributors

Critical Gradient Response of theWeiland Model

JET Energy Confinement in the Hot-Electron Mode

E. Asp[1], J. Weiland[2], X. Garbet[1], V. Parail[3], P. Strand[2]
and JET EFDA contributors*

[1]Association EURATOM -CEA, CEA Cadarache, 13108 St Paul-Lez-Durance, France
[2]Chalmers University of Technology, EURATOM-VR, Göteborg, Sweden
[4]EURATOM/UKAEA Fusion Association, Culham Science Centre, Abingdon, OX14 3DB, UK
[5]Max-Plank-Inst. für Plasmaphysik, IPP-EURATOM, Garching, Germany
** See annex of J. Pamela et al, "Overview of JET Results ",*
(Proc.20 [th] IAEA Fusion Energy Conference, Vilamoura, Portugal (2004).

Preprint of Paper to be submitted for publication in
Plasma Physics and Controlled Fusion

ABSTRACT.
This paper explores the features of the Weiland model as a gyro-Bohm Critical Gradient Model (CGM). The characteristic feature of a CGM is that whenever a threshold value in the temperature gradient is surpassed the transport switches from a low to a high level. In CGM, the reformulated Weiland diffusivities are given by $\chi = \chi^{gB}\,\chi_s(R/L_T - R/L_{T,th})^{\alpha} + \chi^{gB}\,\chi_0$, where α = 1/2–3/2, roughly depending on the height above threshold. In empirical CGM $\alpha = 1$ is the norm, which was shown to hold also for the Weiland model for a wide range of R/L_T at constant threshold. In this paper the critical gradient response of the Weiland model is studied in realistic scenarios where all temperatures and thresholds respond to the increasing heating. It turns out that in this case we are sufficiently far above the threshold to assume $\alpha = 1/2$.

The simulations of the plasma response to increasing electron or ion heating, yield the Weiland model as a stiff model. The change in $(R/L_T - R/L_{T,th})^{1/2}$ is moderate compared to the large variation in the heating powers. A correlation between higher ion stiffness and a stronger trapped electron mode drive of the ion diffusivity, was observed. Heat pinches were shown to distort the evaluation of the background transport and give $\chi_0 < 0$.

1. INTRODUCTION

In this work we have chosen to numerically investigate the reaction of a plasma to increasing ion or electron heating, in order to evaluate the critical gradient behaviour of the Weiland model[1][2][3][4]. The increasing ion heating extrapolates the common neutral beam heated plasma scenario at JET, which pushes the plasma towards more beneficial hot-ion mode[5], from a confinement point of view. In a burning plasma like ITER however, the α-particles produced by the fusion reactions heat the electrons and might create a hot-electron plasma. Thereof the interest for a deeper understanding of the effects of both higher ion and electron power depositions on plasma transport properties.

In the last couple of years a number of experiments have studied heat transport by scans of power deposition profiles or by seeking a relationship between the radial variation of the heat flux and the steepness of the temperature profile [6], [7], [8], [9]. Their findings indicate the existence of a threshold above which the heat diffusivity amplifies and thereby opposes further steepening of the profiles. However, the quantification of these responses is not straight forward in steady-state experiments as several plasma parameters, which are known to affect transport, vary simultaneously with the thresholds and temperatures. Experimentally this can be avoided by power modulation experiments [10], [11], [12]. It should be noted that the steadystate problems have been circumvented in this work by the benefit of freezing parameters and doing numerous simulations. By probing the outcome of each simulation at a specific radius it was made certain that all parameters except the temperatures do not change inbetween simulations when they are compared. The analysis presented here will in other words reveal pure temperature effects.

Currently, a threshold at which the transport switches from a residual to highly turbulent exists in the majority of transport models like RLW [13], IFS-PPPL [14], GLF23 [15], OHE [16], Multi-

Mode [17] and Weiland model. A review of these models is available in [18]. The threshold feature is taken into account in empirical gyro-Bohm Critical Gradient Models (CGM) [19] [20]. Empirical CGM was developed as an analysing tool for gauging the response of the heat transport to different height above thresholds. The on-off mechanism of transport in CGM can lead to plasma parameters staying close to marginal stability, as the induced transport relaxes the plasma towards the threshold. The concept of stiffness is a consequence of this behaviour.

We have here reformulated the Weiland model according to the CGM formalism. This has an interesting implication for the height-above-threshold dependence of the heat diffusivity, as it varies with the distance from the threshold in Weiland CGM. Normally the dependence is assumed to be linear in the Weiland model close to the threshold [21], in conjunction with gyro-kinetics. In the present case, the unstable modes are far from the threshold which instead renders the Weiland diffusivities proportional to square root of the height above threshold. This is not a unique feature of the Weiland model, the gyro-fluid model IFS-PPPL[14] has similar properties. Other relationships than the linear gyro-kinetical have as well been proposed for the heat diffusivities [12].

This study relies on the Weiland model as implemented in JETTO [22]. The effect of the threshold in this model is generally thought to be weaker than in other, similar models [23]. That the threshold nevertheless is important in this model is clearly seen from the behaviour of the ion temperature for increasing electron heating. Indeed, it would not be wise to try to evaluate the heat transport of the Weiland model without knowing the thresholds.

A quantitative measure of stiffness can be calculated if the heat diffusivity and height above threshold responses to increasing heating are considered. If a plasma is stiff there will only be a small change in the height above threshold for a significant change in the heating power. This normally implies a large variation in the heat diffusivity as well. Hence calculating the rate of change of the heat diffusivity with respect to the height above threshold can give an idea of the level of stiffness.

In the electron heating case it is found that ion stiffness varies with the instabilities responsible for the drive of the ion transport (figure 5(b)). At low heating powers, the drive from Ion Temperature Gradient (ITG) mode is dominant, followed by a phase of ITG and Critical Gradient Response of the Weiland Model 3 Trapped Electron (TE) mode driven ion transport. This transition almost triples the stiffness. For the highest electron heating powers, the ions become what could be described as infinitely stiff. The TE mode then strongly drives the ion transport. For higher ion heating, the ITG mode remains dominant and the stiffness is comparable to the case of low electron power (figure 6). Analysis of the simulations using the empirical CGM gives evidence of the Weiland model being quite stiff contrary to previous results [23]. That the Weiland model is capable of satisfyingly reproducing stiff plasmas, has been shown by modelling of JET discharges [31].

In the Weiland CGM, extrapolation of the diffusivities down to the threshold gave negative ambient diffusivities. This is not an effect of the varying dependence on the height above threshold in the Weiland model, but is rather due to pinches distorting the transport close to the threshold. Hence, a CGM should be used with care close to the threshold.

We begin this paper by an introduction of the temperature dependent aspects of the Weiland model in section 2. The CGM version is also derived in this section. The method and simulations are presented in section 3, the results in section 4 with an evaluation of CGM response in 5. This paper ends with conclusions in 6.

2. THE WEILAND MODEL

In this section we briefly describe theWeiland model. The equations displayed only holds the main features of the model and are used as a simple tool to gain a better understanding of how the plasma responds to the heating scenarios of the next section. The various ways of how electron and ion properties can influence the transport of the other species are also addressed.

2.1. THE INSTABILITY OF ITG AND TE MODES

In essence the reactive drift modes of the Weiland model are interchange modes arising from the pressure inhomogeneity with gravity replaced by the centrifugal force experienced by the particles as they follow the twisted magnetic field lines. Reactive drift modes arise if particle trapping inhibits quasi-neutrality or if a temperature gradient causes a competition between convection and thermalisation [26] [27]. Here the stability of Trapped Electron (TE) and Ion Temperature Gradient (ITG) modes are studied. The numerical version of the Weiland model used here also includes impurity ITG modes and electromagnetic effects. In the most basic version of the Weiland model for toroidal geometry and circular, concentric magnetic surfaces the dispersion relation is given by [4],

$$\begin{aligned}
&\frac{\omega_{*e}}{N_i}\left[\omega\left(1-\frac{2L_{ni}}{R}\right)+\left(\frac{L_{ni}}{L_{Ti}}-\frac{7}{3}+\frac{10}{3}\frac{L_{ni}}{R}\right)\omega_{Di}\right.\\
&\left.-k_\theta^2\rho_s^2(\omega-\omega_{*iT})\left\{\frac{\omega}{\omega_{*e}}+\frac{10}{3}\frac{T_i}{T_e}\frac{L_{ni}}{R}\right\}\right] \qquad (1)\\
&=f_t\frac{\omega_{*e}}{N_e}\left[\omega\left(1-\frac{2L_{ne}}{R}\right)+\left(\frac{L_{ne}}{R}-\frac{7}{3}+\frac{10}{3}\frac{L_{ne}}{R}\right)\right]\omega_{De}+1-f_t
\end{aligned}$$

where the resonance factor

$$N_{e,i}=\omega^2-\frac{10}{3}\omega\omega_{De,i}+\frac{5}{3}\omega_{De,i}^2 \qquad (2)$$

Above ω is the complex mode frequency, subscripts e and i denote electrons and ions respectively, T is the temperature, ω_* is the diamagnetic drift frequency, ω_{*iT} is the ion diamagnetic drift frequency of the full pressure gradient, ω_D is the magnetic drift frequency, k_θ is the poloidal mode number, ρ_s is the ion Larmor radius at the electron temperature, f_t is the fraction of trapped particles, R is the major radius, and

$$L_T = -\frac{d\,\mathrm{In}\,T}{dr} \quad \text{and} \quad L_n^{-1} = -\frac{d\,\mathrm{In}\,n}{dr} \tag{3}$$

with *r* as the minor radius and *n* as the particle density.

The dispersion relation (1) of the ITG and TE modes decouple if the density profile is flat enough, i.e. if $R/L_{ne} < 2$. In this case the complex frequency of the ITG mode is given by the real frequency,

$$\omega_{ri} = \frac{k_\theta \rho_s}{2L_{ni} m_i^{1/2}} T_e^{1/2} \left[1 - \frac{2L_{ni}}{R}\left(1 + \frac{10}{9}\,\frac{T_i}{T_e}\right)\right] \tag{4}$$

and the growthrate,

$$\gamma_i = \frac{2^{1/2} k_\theta \rho_s}{R m_i^{1/2}}\, T_e^{1/2} \sqrt{\frac{R}{L_{Ti}} - \frac{R}{L_{Ti,th}}}\,, \tag{5}$$

with threshold

$$\frac{R}{L_{Ti,\,th}} = \frac{2}{3}\frac{R}{L_{ni}} + \frac{20}{9}\frac{T_i}{T_e} + \frac{1}{2}\left[1 - \frac{R}{L_{ni}} + \frac{1}{4}\left(\frac{R}{L_{ni}}\right)^2\right]\frac{T_e}{T_i}\,, \tag{6}$$

in which the finite Larmor radius correction has been neglected for simplicity. In the limit $R/L_{ni} = 2$ the third term of the ion threshold vanishes. This is the case of the shot studied here, which has $R/L_{ni} = 1.8$. Thus the effective threshold becomes,

$$\frac{R}{L_{Ti,th}} \approx \frac{2}{3}\frac{R}{L_{ni}} + \frac{20}{9}\frac{T_i}{T_e}\,, \tag{7}$$

and its only remaining temperature dependence is inversely proportional to T_e/T_i. The threshold will thus never start to increase and improve confinement at large T_e/T_i. The trapped electron part of the dispersion relation (1) yields in the uncoupled case the real frequency,

$$\omega_{re} = -\frac{k_\theta r_s}{2L_{ne} m_i^{1/2}}\, T_e^{1/2} \left[K_t\left(1 - \frac{2L_{ne}}{R}\right) - \frac{20}{3}\,\frac{L_{ne}}{R}\right] \tag{8}$$

and growthrate,

$$\gamma_e = \left(\frac{2K_t}{m_i}\right)^{1/2} \frac{k_\theta \rho_s}{R}\, T_e^{1/2} \sqrt{\frac{R}{L_{Te}} - \frac{R}{L_{Te,th}}}, \tag{9}$$

with threshold

$$\frac{R}{L_{Te,th}} = \frac{20}{9K_t} + \frac{2}{3}\frac{R}{L_{ne}} + \frac{K_T}{2}\left[1 - \frac{R}{L_{ne}}\right]^2 \tag{10}$$

and the ratio of trapped to free electron, $K_t = f_t/(1-f_t)$.

The main thing to notice regarding the pure trapped electron mode depicted above is that it only depends on electron parameters. This is in contrast to the pure ion temperature gradient mode, which depends on electron properties as well. Hence, if the TE mode responds to a change in the ion part of the plasma, it has to be due to linear mode coupling from (1). For ITG modes the amplitude factor of equation (5) and the threshold (7) can counteract each other when T_i rises. The higher threshold can suppress the growth of γ_i and results in the improved confinement properties of the hot-ion mode.

2.2. ION TEMPERATURE RESPONSE TO ELECTRON HEATING

In the ensuing simulations the full Weiland model is used to predict the responses of the temperature profiles to the stronger electron or ion heating. In JETTO, which is the code used for the simulations, the effective heat diffusivity is given by the summation over all unstable modes. Somewhat simplified this sum is given by,

$$\chi_{e,i} = f_{e,i}\,\frac{2m^{1/2}}{k_\theta \rho_s e^2 B^2 R}\,T_e^{3/2}(\mathrm{eV})\sum_{\gamma>0}\frac{\gamma^3}{(\omega_s \mp \frac{5}{3}\frac{T_{ei}}{T_e})^2+\gamma^2} \qquad (11)$$

where $f_e = f_t$, $f_i = 1$, $\hat{\omega}_r$ and $\hat{\gamma}$ are normalised to the magnetic drift frequency of the electrons. It is also assumed that the radial correlation length is of the same order as the poloidal one, i.e. $k_r^2 \approx k_\theta^2 = 0.1/\rho_s^2$. This derives from $k_\theta^2\rho_s^2 = 0.1$ for the most unstable modes [23]. The employed JETTO version uses this constant value and hence it is regarded as fixed in the analytical expressions too. A recent version of the Weiland model includes the effects of magnetic shear on the correlation length and changes the condition $k_\theta^2\rho_s^2 = 0.1$ accordingly[24].

The largest contribution to the sum (11) originates from the mode with the smallest resonance factor, $\hat{\omega}_r \pm 5T_{e,i}/3T_e$. The resonances usually occur at the ITG frequency for the ion diffusivity and at the TE frequency for the electron diffusivity. Nevertheless the T_i/T_e factor in the resonance has interesting implications for the ion transport as it allows more equal coupling to the TE mode at large values of T_i/T_e, where the second term of the resonance $\hat{\omega}_r \pm 5T_{e,i}/3T_e$ becomes negligible. This is particularly true when the electron heating reaches considerable values. This boost of the ion heat diffusivity without the heating to balance it most likely leads to a drop in the ion temperature.

In general, $\chi_{e,i} \propto \hat{\gamma}_{e,i}^{\alpha}$ with $\alpha = 1$ to 3 depending on the relative magnitudes of $(\hat{\omega}_r \pm 5T_{e,i}/3T_e)^2$ and $\hat{\gamma}_{e,i}^{\alpha}$ [21]. It is thus important to investigate in which regime the transport is before determining the value of . If the resonances in equation (11) are strong, a mixinglength estimation can be used to evaluate the diffusivities which yields

$$\chi_i = \frac{\gamma_i}{k_r^2} \propto T_e\,T_i^{1/2}\sqrt{\frac{R}{L_{Ti}}-\frac{R}{L_{Ti,th}}}\cdot H\left(\frac{R}{L_{Ti}}-\frac{R}{L_{Ti,th}}\right) \qquad (12)$$

$$\chi_e = f_t \frac{\gamma_e}{k_r^2} \propto T_e^{3/2} \sqrt{\frac{R}{L_{Te}} - \frac{R}{L_{Te,th}}} \cdot H\left(\frac{R}{L_{Te}} - \frac{R}{L_{Te,th}}\right) \tag{13}$$

where H is the Heaviside function ensuring that only unstable modes drive transport in conjunction with the sum in equation (11).

From equation (12) it is easy to see why T_i drops when T_e rises as the ion threshold (7) then lowers. Together with the T_e dependence of the amplitude, these effects amplify χ_i. For constant ion heating power, more heat is expelled than absorbed and the ion temperature decreases, suppressing the ITG threshold even further. Luckily, the increased transport also works to shrink R/L_{Ti}, which reduces the augmentation of transport. It is this stiffness feature of χ_i that prevents it from growing out of proportion, completely depleting the ion energy. Together with the TE mode drive of ion transport this can explain the decrease of the ion temperature for increasing electron heating, not only observed in these simulations but also in experiments at DIII-D[28] and ASDEX Upgrade [29].

2.3. WEILAND CGM

For easy evaluation of transport in experiment, the empirical gyro-Bohm critical gradient model was developed [19]. It basically determines the transport through three numbers describing the instability threshold and the levels of anomalous and ambient transport. The number for the anomalous transport has been used to evaluate the stiffness of plasmas, giving a quantitative measure for comparison between discharges and machines [20]. Rewriting equations (12) and (13) in CGM manner while retaining the square root dependence of the height above threshold, yields

$$\chi_i = \chi_i^{gB} \chi_{si} \sqrt{\frac{R}{L_{Ti}} - \frac{R}{L_{Ti,th}}} \cdot H\left(\frac{R}{L_{Ti}} - \frac{R}{L_{Ti,th}}\right) + \chi_i^{gB} \chi_{0i} \tag{14}$$

and

$$\chi_i = f_t \chi_i^{gB} \chi_{se} \sqrt{\frac{R}{L_{Te}} - \frac{R}{L_{Te,th}}} \cdot H\left(\frac{R}{L_{Te}} - \frac{R}{L_{Te,th}}\right) + \chi_e^{gB} \chi_{0e} \tag{15}$$

with

$$\chi_i^{gB} = \frac{T_e^{1/2} T_i^{1/2} \rho_s}{eBR} \quad \text{and} \quad \chi_e^{gB} = \frac{T_e \rho_s}{eBR} \tag{16}$$

and

$$\chi_{si}^{gB} = \frac{2^{1/2}}{k_\theta \rho_s} = 4.7 \quad \text{and} \quad \chi_{se} = \frac{2^{1/2}}{k_\theta \rho_s} \frac{f_t^{1/2}}{(1 - f_t)^{1/2}} = 3.2 \tag{17}$$

for the fastest growing mode with $k_\theta^2 \rho_s^2 = 0.1$, and $f_t = \{2r/R/(1+r/R)\}^{1/2}$ with $r/R = 0.2$. This corresponds a normalised minor radius, $r/a = \rho = 0.6$ where the heat transport analysis will take place. The second term in equations (14) and (15) represents the contributions from the instabilities far from the resonance $\omega_r \pm 5T_{e,i}/3T_e$ in equation (11). In the simulations χ_{0i} and χ_{0e} also include neoclassical transport.

In the investigation of the $(R/L_T - R/L_{T,th})^\alpha$ dependence in the original work by F. Imbeaux et al [19], $\alpha = 1$ only gave a slightly better fit to the experimental data than $\alpha = 1/2$. As that study was performed close to the threshold, it is not inconsistent with $\alpha = 1/2$ far from the threshold in the Weiland CGM presented above. In IFS-PPPL the criterion for is given by the minimum value of $(R/L_T - R/L_{T,th})$ and $(R/L_T - R/L_{T,th})^{1/2}$, i.e. for values larger than unity $\alpha = 1/2$.

Since in empirical CGM was derived for $\alpha = 1$, it is hard to compare the stiffness levels obtained from experiment with the ones given by equations (14) and (15) above. We may still compare the χ_s numbers given by the slope of the curve χ/χ^{gB} vs $(R/L_T - R/L_{T,th})^{1/2}$, between simulations to get an idea of if electron or ion heating renders the model more stiff and study how much $(R/L_T - R/L_{T,th})^{1/2}$ changes when more heating is applied.

3. SIMULATIONS OF PLASMA RESPONSE TO INCREASING HEATING

The simplest way of varying the height above threshold is to make a scan over the minor radius. The problem with this approach is that several parameters affecting transport are also radially dependent. It might thus be hard to separate different effects from one another. To avoid this problem, the transport can be evaluated at a single radial value but it requires several similar, preferably identical plasmas. Experimentally this can be hard to obtain, and hence two series of simulations have been carried out varying either the electron or ion power of JET Pulse No: 50628 [30] at time = 10s (fig.1). Note that in figure 1(a) the ion temperature decreases with higher electron heating and that in figure 1(b), the electron temperature rises only slightly when the ion heating increases. Although the plasma current was allowed to evolve in addition to the temperatures in the simulations, it was unaffected by the increasing heating and hence the transport becomes a function of the temperatures only.

Usually the Weiland model in JETTO is considered to be valid within $0.2 < \rho < 0.8$, where ρ is the normalised minor radius. The two bottom panels of figures 1(a) and 1(b) displaying $R/L_{Te,i}$, show that the largest variation of the temperature inhomogeneities occurs outside $\rho = 0{:}8$. This region is dominated by non-stiff neoclassical transport. So, even if the outer boundary condition is frozen at $\rho = 1$, the boundary changes where theWeiland validity region begins at $\rho \approx 0{:}8$. Hence, it is not expected that the temperature profiles in each of the second and third panels of 1(a) and 1(b) have to coincide, as might be concluded from a stiff model. Moreover, in a stiff model with a changing threshold, the profiles have to adjust accordingly, like the dropping ion temperatures in figure 1(a).

4. PREDICTED HEAT FLUX RESPONSES TO INCREASING HEATING

In this paper the normalised value, $\rho = 0.6$, of the minor radius has been chosen to evaluate the influence of the changing temperature profiles at constant plasma parameters. Most of the heating

power has been absorbed inside this radial value (uppermost panel of 1(a) and 1(b)), which is well within the validity region of the Weiland model.

The use of the mixing-length estimates (12) and (13) to determine the CGM behaviour is justified for these simulations as $(\omega_r \pm 5T_{e,i}/3T_e)^2$ is sufficiently small compared to γ^2. This is especially true for the electrons and at higher heating powers.

The curves in figures 2(a), 2(b), 3(a) and 3(b) show signs of the existence of a threshold above which anomalous transport becomes significant. In this case the threshold of each mode is extracted by scanning L_{Te} or L_{Ti} in a stand-alone version of the Weiland code. When the growthrates exceed a critical value, the thresholds in figure 4 are obtained. These figures show R/L_T values well above threshold, far from marginal stability. Similar observations were made in ASDEX Upgrade, with comparison of experimental profiles and theoretical TE thresholds from the Weiland model[32].

The discontinuities in figures 2(d) and 4(b) are due to the fact that a stand-alone version of theWeiland model is used for the calculation of the thresholds in all $R/L_T - R/L_{T,th}$. The thresholds are not explicitly calculated and therefore they cannot be extracted directly from JETTO. For some reason the stand-alone code overestimates the thresholds and completely suppresses the ITG mode for strong electron heating whereas in JETTO, they only diminish (figure B1(b)). This descrepancy between the two codes results in the discontinuities in figures 2(d) and 4(b). Although overestimated, the thresholds in the stand-alone code, show the same trend as theory (figure 4(b)) and thus it should not affect the evaluation of the CGM behaviour.

Figures 2(c), 2(d), 3(c) and 3(d) display the heat flux response to the height above threshold, for increasing electron or ion heating power, respectively. The impact of the thresholds is important and can be most easily observed in the ion heat flux in the electron heating case. The strange shape of 2(b), where R/L_{Ti} becomes smaller for higher values of qi is due the ITG threshold (7) which decreses with the larger T_e/T_i. The lower threshold amplifies the ion diffusivity. Since no heating is applied to the ions in this case, this leads to a depleation of ion energy and to that the ion temperature drops and flattens. The strange shape of qi in figure 2(b) is therefore the consequence of an infinitely stiff ion response where R/L_{Ti} follows the lower thresholds in figure 4(b) and keeps $R/L_T - R/L_{T,th}$ constant in figure 2(d) for high electron heating.

From the basic model in section 2.1 the electron heat flux in figure 2(a) should not respond at all to the ion heating. The reason ion heating affects the electrons is in this case due to thermal equilibration, see Appendix A. Experimental findings at JET by P. Mantica et al [33] show higher electron stiffness with increasing ion heating. There are two possible explanations to this. Firstly, the density profiles in these experiments are peaked and this makes it impossible to separate the dispersion relation (1) into pure ITG and TE modes. Ion properties may then directly influence the TE mode. Secondly the density in the experiments by Mantica et al is larger than here, $5\times10^{19}\mathrm{m}^{-3}$ compared to $4\times10^{19}\mathrm{m}^{-3}$. The thermal equlibration scales as the density squared, so it would be likely it plays an even stronger role in the experiments by Mantica than in our modelling.

5. WEILAND CGM ANALYSIS

As was shown in the previous section the plasma response has stiff properties. In order to quantify the stiffness in this study and enable a comparison between the two heating scenarios or even within a heating scenario, the CGM introduced in section 2.3 was put to use. In figures 5 and 6 the values of χ_s are calculated. The major difference between the two heating schemes Critical Gradient Response of the Weiland Model 9 is that the plasma gets stiffer for higher electron heating with an increasing χ_s as a result. Ion heating seems not to make the plasma stiff to the same extent as electron heating. The change of s in the electron heating case coincides well with the type of instabilities present and their influence on the diffusivities through equation (11). In figure 5(b) the χ_{si} = 10, 27 and 153 derives from situations when the diffusivity is ITG dominated, is driven equally by ITG and TE and then becomes mostly TE excited, respectively. As discussed in section 2.2 and shown in Appendix B, the ion diffusivity goes through these phases as T_e/T_i increases since the ITG mode subsides and TE mode gains significance in the ion part of the sum (11). The change in se from 4.4 to 14 in figure 5(a) coincides with the TE mode dominance of i. It is interesting to note that for low $R/L_T - R/L_{T,th}$ in the electron heating case, the stiffness numbers are comparable to the ion heating case in which the ITG mode dominates throughout the heating interval.

Although considered a non-stiff, the Weiland model has successfully reproduced power modulation experiments in ASDEX Upgrade [25] and JET [31]. The χ_s values quoted above behave in a way consistent with what would be expected from a CGM model, but cannot be compared with experimental s calculated with the empirical CGM. For a large variation in the applied power the, 0–38.5MW and 0–28MW in the electron and ion heating case respectively, only short ranges (0:6) of $(R/L_T - R/L_{T,th})^{1/2}$ are obtained. The plasma seems also in most cases to react to higher deposited power with smaller changes in the height above threshold. To get a definite measure of the stiffness of the Weiland model the empirical CGM was employed in Appendix C. With $\chi_{se}^{emp} \approx 0.7 - 2$ and $\chi_{si}^{emp} \approx 2 - 31$, these simulations would have been regarded as stiff, had they been real experiments.

5.1. PINCH EFFECTS

The curves in figures 5 and 6 imply that the diffusivities are negative at the threshold where they are expected to be neoclassical. The large negative values are partly due to the fact that closer to the threshold the diffusivities are more proportional to γ^3 thanγ. Hence, a cubic fit for the smallest values of χ should correct this. Figure 7 certainly shows an improvement, but χ_e is still negative.

Negative values of the diffusivities are usually due to pinches, which add a factor to the diffusivities in section 2 and, schematically,

$$\chi^{\text{pinch}} = \propto \frac{\mathrm{R/L_{Ti}} - (\hat{\omega}_r, \mathrm{R/L_n})}{\mathrm{R/L_{Ti}}} \cdot \frac{(\mathrm{R/L_T} - \mathrm{R/L_{T,th}})^{3/2}}{\mathrm{R/L_T} - \mathrm{R/L_{T,th}} + \Delta(\hat{\omega}_r, \mathrm{R/L_n})^{3/2}}, \tag{18}$$

where the functions $p(\omega_r, R/L_n)$ and $\Delta(\omega_r, R/L_n)$ represent pinch effects and the resonance in equation

(11), respectively. For the ions, these functions also includes T_e/T_i and R/L_{Te} dependencies (see e.g. reference [3]). Generally, larger pinch terms have a tendency to flatten the diffusivity for small $(R/L_T - R/L_{T,th})^{1/2}$ and then make the diffusivity negative when $p > R/L_T$. Bigger Δ's have a similar effect, except they cannot make $\chi < 0$. The influence of varying the thresholds is more marginal, but can affect the importance of the pinch.

Figure 8 illustrates the effects of the pinch for an electron-like 8(a) and an ion-like case 8(b). The electron-like case has a pinch, $p = 3.25$ and resonance term, $\Delta = 0.1$, whereas the ion-like case has p = 0:25 and Δ = 1:5. These figures are adjusted to the TE threshold used, $R/L_{T,th} = 1.9$. Since we from figure 7 expect the pinches to be important for the electrons and of less significance for the ions, the values of p were chosen accordingly.

The figures 8(a) and 8(b) yield that the linear fits are inaccurate closer to the threshold. Also the cubic fits fail in this region, underestimating the diffusivity in the electron case and overestimating it in the ion case. This agrees qualitatively with the results from the cubic fits in figure 7. It is thus important to keep in mind that the ambient transport can be distorted by pinch effects when doing CGM analysis.

CONCLUSIONS

Compared to an empirical gyro-Bohm Critical Gradient Model (CGM), the Weiland model have a somewhat different behaviour. The in CGM linear dependence on the height above threshold, $R/L_T - R/L_{T,th}$, becomes in theWeiland model $(R/L_T - R/L_{T,th})^{\alpha}$, with $\alpha = 1/2 - 3/2$ depending on the distance to the threshold. The performed simulations show, in this case, that we are sufficiently above the threshold to assume that square root dependence on the height above threshold is the most accurate one.

The importance of the threshold when evaluating stiffness through CGM, is most easily perceived in the ion heat flux response to electron heating. For high electron heating, the ion temperature profile flattens to follow the shrinking ITG threshold. Without this information on the threshold, it might be concluded that the ion response is not stiff, when indeed the opposite is true. It is the stiffness of the ion temperature that forces it to drop. To avoid rash conclusions, the threshold always has to be taken into account when determining the stiffness of a plasma.

Quite stiff features of theWeiland model were found in the analysis of simulations of the plasma response to increasing electron and ion heating. This was not expected as previous comparison to other transport models, especially gyro-kinetic or gyro-fluid, revealed the Weiland model as less stiff and it has since been considered non-stiff. On the other hand, the Weiland model has performed well in modelling heat modulation experiments. The plasma response gets stiffer for higher electron heating, with smaller changes in the height above threshold for larger variations in the heating power. This is reflected in the increase of the calculated stiffness numbers for higher electron heating.

A clear correlation between higher ion stiffness and stronger drive from the Trapped Electron (TE) mode of the ion diffusivity was observed. For low electron to ion temperature ratios, T_e/T_i, the

Ion Temperature Gradient (ITG) mode is mainly responsible for the ion diffusivity. As T_e/T_i increases the impact of the TE mode becomes non-negligible. This extra diffusivity drive pushes the ion temperature profile down towards marginal stability which makes the ions react in a stiffer manner.

Caution is required when estimating the ambient, neoclassical transport by CGM analysis. The, in CGM neglected, pinch factor in the anomalous transport creates an offset between the real and CGM diffusivities. The result of this offset is that CGM analysis underestimates the ambient transport. According to the version of theWeiland model without pinches, the diffusivities should scale like $(R/L_T - R/L_{T,th})3=2$ close the the threshold. Comparison of a fit of this kind to the full expression with pinches, reveals that the electrons are influenced by a strong pinch, whereas the ions have a more moderate pinch.

The drop and a flattening of the ion temperature profile is observed when the electron heating increases at constant applied ion power. To begin with this effect is not significant as the thermal exchange power provides the ions with a sufficient amount of extra energy. That the ion temperature decreases is not at all surprising since the ITG mode of the Weiland model contains a feedback loop which continuously amplifies the ion heat diffusivity when the electron temperature rises. The feedback loop is broken when the ion diffusivity reaches such levels it keeps the ITG mode close to marginal stability. At this point the TE mode becomes significant for the drive of ion heat transport.

Contrary to expectations, the electron temperature responds to increasing ion heating. Again this is an effect of the thermal exchange power, effectively heating the electrons and has little to do with a coupling of the TE and ITG modes. The latter is not expected in this case, as the plasma has a density profile flat enough to decouple ITG and TE modes.

In summary the Weiland model has somewhat different features than empirical CGM and contrary to common belief it can be quite stiff. Two points would make it interesting to redo the experiments that resulted in the empirical CGM using ion instead of electron power modulation. Firstly, according to the Weiland model the ion gyro-Bohm diffusivity can contain both the electron and ion temperature. The temperature will still appear as a factor $T^{3/2}$ but how it is divided between the ion and electron temperature depends on the distance from the threshold. That leads us to the second point. The exponent of the ion temperature is the same as the exponent for the height above threshold. Hence, if for instance fits with $\alpha = 1/2$ and $\alpha = 1$ for the height above threshold give equal results, it would be possible to distinguish them by the fit of the ion temperature. In the electron modulation case this is not possible as the electron gyro-Bohm diffusivity depends solely on the electron temperature. Until now the capabilities of measuring the ion temperature in ion power modulation experiments have been too poor to give sufficient resolution, but with recent upgrades in JET the possibility of a successful experiment is high.

REFERENCES

[1]. Guo S.C. and Weiland J., Phys. Fluids **37** (1997) 1095

[2]. Jarmen A. *et. al*, Nuclear Fusion **27** (1987) 941

[3]. Nordman H. *et. al*, Nuclear Fusion **30** (1990) 983
[4]. Weiland J., Collective modes in inhomogeneous plasma, IOP Publishing Ltd (2000)
[5]. JET Team, Nuclear Fusion **39** (1999) 1619
[6]. Ryter F. *et. al*, Phys. Rev. Lett. **86** (2001) 2325
[7]. Hoang C. *et. al*, Phys. Rev. Lett. **87** (2001) 125001
[8]. Mikkelsen D.R. *et. al*, Nuclear Fusion **8** (2003) 30
[9]. Wolf R.C. *et. al*, Plasma Phys. Control. Fusion **45** (2003) 1757
[10]. Ryter F. *et. al*, Nuclear Fusion **43** (2003) 1396
[11]. Mantica P. *et. al*, in proceedings of the 19th IAEA Fusion Energy Conference, Lyon (2002)
[12]. Peeters A.G. *et. al*, Phys. Plasmas **12** (2005) 022505
[13]. Rebut P.H., Lallia P.P. and Watkins M.L., in Plasma Physics and Controlled Nuclear Fusion Research, Proceedings of 12th Int. Conf. Nice, 1988, Vol II, IAEA, Vienna (1989) 191
[14]. Kotschenreuther M. *et. al*, Phys. Plasmas **2** (1995) 2381
[15]. Waltz R.E. *et. al*, Phys. Plasmas **4** (1997) 2482
[16]. Ottaviani M., Horton W. and Erba M., Plasma Phys. Control. Fusion **11** (1997) 1461
[17]. Zhu P. *et. al*, Phys. Plasmas **7** (2000) 2898
[18]. ITER Expert Groups on Confinement and Transport and Confinement Modelling Database, Nucl. Fusion 39 (1999) 2175
[19]. Imbeaux F. *et. al*, Plasma Phys. Control. Fusion **43** (2001) 1503
[20]. Garbet X. *et. al*, Plasma Phys. Control. Fusion **46** (2004) 1351
[21]. Heikkilä A. and Weiland J., Phys. Fluids B**5** (1993) 2043
[22]. Strand P. *et. al*, Nucl. Fusion **38** (1998) 545
[23]. Dimits A.M. *et. al*, Phys. Plasmas **7** (2000) 969
[24]. Weiland J. and Holod I. Phys. Plasmas **12** (2005)
[25]. Ryter F. *et. al*, Nucl. Fusion **41** (2001) 537
[26]. Liu C.H., Phys. Fluids **12** (1969) 1489
[27]. Rudakov and Sagdeev Sov. Phys. Doklady **6** (1961) 415
[28]. McKee G. *et. al*, in proceedings of APS(DPP) meeting, Long Beach, CA (Oct 2001)
[29]. Manini A. *et. al*L, Europhysics Conf. Abstr. **27A** (2003) P1-127
[30]. Suttrop W. *et. al*, Europhysics Conf. Abstr**. 25A** (2001) 989
[31]. Mantica P. *et. al*, Europhysics Conf. Abstr. **28G** (2004) P-1.153
[32]. Tardini G. *et. al*, Nucl. Fusion **42** (2002) L11
[33]. Mantica P. *et. al*, in proceedings of the 20th IAEA Fusion Energy Conference, Vilamoura, Portugal (2004) EX/P6-18

APPENDIX A. EFFECTS OF THERMAL EQUILIBRATION

As can be seen from figures 1(b) and 3(a) electron properties react to the increasing ion heating. Although the absorbed electron heating is constant, the effective heating,

$$P_e^{eff} = P_e^{abs} - P_{rad} - \frac{\partial W_{th,e}}{\partial t} - P_{THX} \tag{A.1}$$

changes. Here P_e^{abs} is the heating absorbed by the electrons, P_{rad} is the impurity radiation, $W_{th,e}$ is the thermal energy content of the electrons and $P_{THX} \propto T_e - T_i$, arises from thermal equilibration. In the presented case, P_{THX} is the source of variation in Pee which effect on the electron temperature is shown in figure A1(a). That the electrons and ions do not communicate widely through a coupling effect of ITG and TE modes can be seen from figures 4(c) and 2(b) as neither the TE threshold nor growth rate show any considerable dependence on $T_e - T_i$.

The effect of higher T_e on T_i is not very big for low electron heating. The difference in T_i between the zeroth and 100th percent heating levels of figure 1(a) is negligible and only a minor drop can be seen at the 300% level. At electron heating powers upto about 11MW (200%) the effect of thermal equilibration is so strong it can counteract the ion temperature's natural tendency to decrease. As can be seen from figure A1(b) the effective ion power increases and keeps T_i at a constant level for some time until the trapped electron drive forces it to drop.

APPENDIX B. MODE IDENTIFICATION

As discussed in section 2.2, all unstable modes are, to different degrees, responsible for the heat fluxes in figures 2(a), 2(b), 3(a) and 3(b). To better understand the underlying physics it is important to try and resolve which modes drive the ion and electron transport. This mainly concerns the ions as χ_i (11) contains a T_e/T_i dependence that can increase the influence of the TE mode. In a more up-to-date version of JETTO this is a straight forward task, since the real part of the frequency can be used to distinguish modes from one another. Here a more rudimentary, but efficient, method is used.

In figures B1 and B2 a simple comparison between growthrates and diffusivities are made. The diffusivities (12) and (13) are normalised using the electron temperature and should hence be directly proportional to the growth rates (5) and (9). The case of ion heating in figure B2 is trivial. The highest growth rate in B2(b) is a perfect match for $\chi_i = T_e$ in B2(a) and the the lower growth rate coincides with $\chi_e = T_e$. That the smallest growth rate shows little dependence on T_e/T_i only strengthens this conclusion.

For stronger electron heating there is one growth rate monotonically increasing with the temperature ratio in figure B1(b) and it seems to drive the electron diffusivity in figure B1(a). The ion diffusivity which first increases and then flattens out, appears to be driven by a combination of both growth rates. Thus the conclusion is that the monotonically increasing belongs to the trapped electron mode, whereas the other belongs to the ion temperature gradient mode. As R/L_{Te} steepens faster than the TE threshold rises in figure 4(a), γ_e is expected to grow with T_e/T_i.

The behaviour of the ITG mode in figure B1(b) can be understood from figure 2(d). The ion heat flux increases steady with the height above threshold until it becomes extremely stiff. This first phase derives from the slowly rising ITG growth rate, for which the threshold, figure 4(b), has started to decrease but the ions are not yet stiff enough to follow. As the ions become stiffer R/L_{Ti} shrinks which accounts for the smaller growth rate at high T_e/T_i. It seems the transition from moderately to extremely stiff ion response coincides with the stronger influence of the TE mode. At this point the ITG threshold is also made higher than the theoretical value (6) as if to adjust the ITG driven heat flux, see figure 4(b).

The conclusions drawn in both the electron and ion heating investigations of figures B1 and B2, are supported by the local code calculating the thresholds.

APPENDIX C. THE EMPIRICAL GYRO-BOHM CRITICAL GRADIENT MODEL

The empirical gyro-Bohm critical gradient model in [19][20] was derived based on the assumptions of a electrostatic gyro-Bohm scaling law, and the existence of an instability threshold with a finite transport below it. After comparison with experiment it was deduced that the best fit of these parameters yielded the thermal diffusivity,

$$\chi = \chi_s \, q^{3/2} \, \frac{T\rho_s}{eBR} \left(\frac{R}{L_T} - \frac{R}{L_{T,th}} \right) H\left(\frac{R}{L_T} - \frac{R}{L_{T,th}} \right) + \chi_0 \, q^{3/2} \, \frac{T\rho_s}{eBR} \qquad \text{(C.1)}$$

where q is the safety factor and H is the Heaviside function. Hence the transport is described by the three parameters χ_s, χ_0 and $R/L_{T,th}$, which can be determined experimentally. It should be noted that these parameters are not constants but depends in turn on other plasma parameters like e.g. T_e/T_i.

The main differences between equation (C.1) and the Weiland versions (14) and (15) are the dependence on q and the linear proportionality to the height above threshold. The former was included in the empirical CGM as to account for improvement of confinement with the plasma current. The linear height above threshold dependence was obtained experimentally studying electron cases close to marginal stability. It is thus not in contradiction to theWeiland CGM in section 2.3, which is valid far above the threshold.

For easy comparison of the degree of stiffness in different plasmas, it is useful to have a quantitative measure of it. In the case of the empirical CGM above, the stiffness number, χ_s, is used to gauge the stiffness of different plasmas[20]. Normally, a $\chi_s > 1$ is regarded as stiff. Despite that equation (C.1) should give a poorer description of the performed simulations than equations (14) and (15) it is an interesting exercise since we can directly compare the empirical χ_s number with the stiffness criterion.

Figure C1 shows the obtained plasma responses in empirical CGM for increasing electron heating (to be compared with figure 5). The obtained stiffness numbers are $\chi^{emp} = 0.7 - 2$ and $\chi^{emp} = 2 -$

31, both large enough to be considered stiff. In experiment χ_{se} has been measured up to 4 [20]. Note that in this formalism, the background ion transport is positive when extrapolating down to the threshold. This holds true also for the ion heating case, although not shown here.

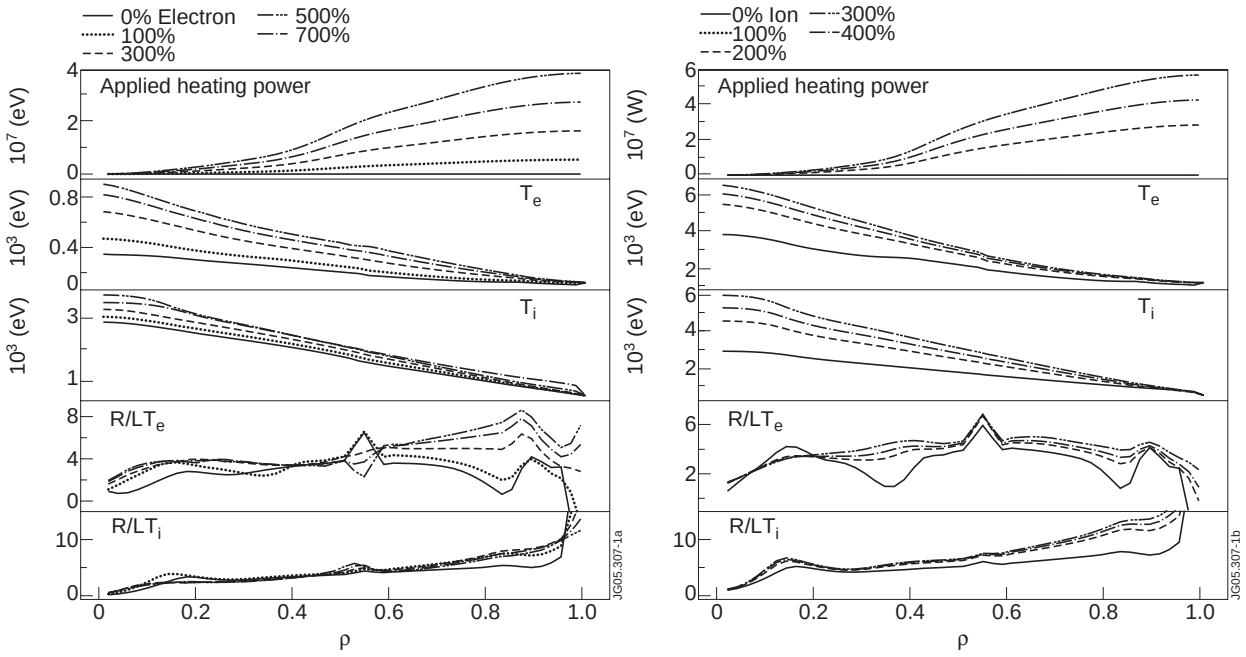

Figure 1. Profile changes in shot 50628 at time=50s for either increasing electron power at constant ion power (a) or vice versa (b). The 100% levels of the heating are 5.5MW and 7MW for the electrons and ions, respectively. Not all profiles are shown to improve visibility.

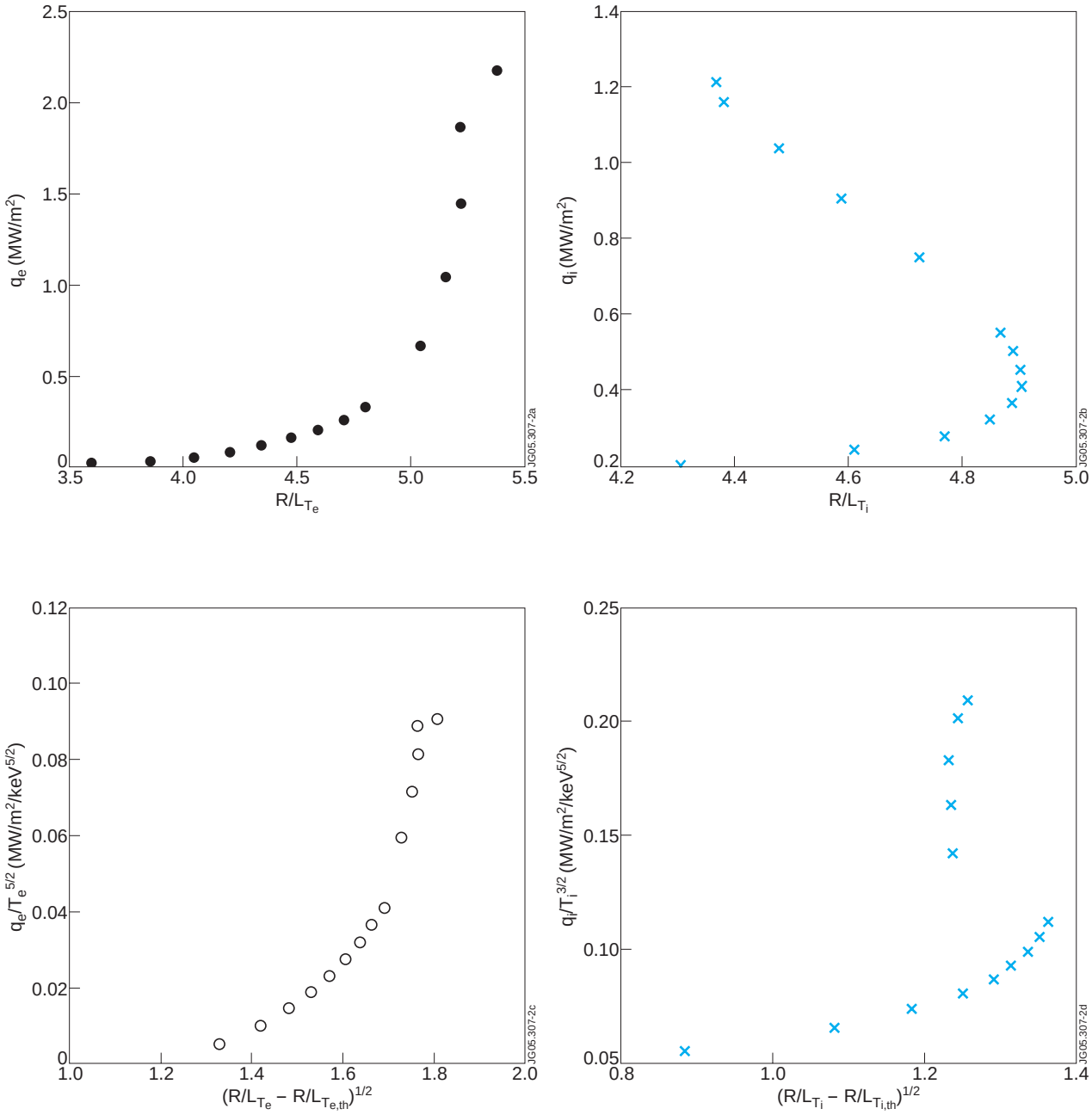

Figure 2. Heat flux responses and stiffness for increasing electron heating.

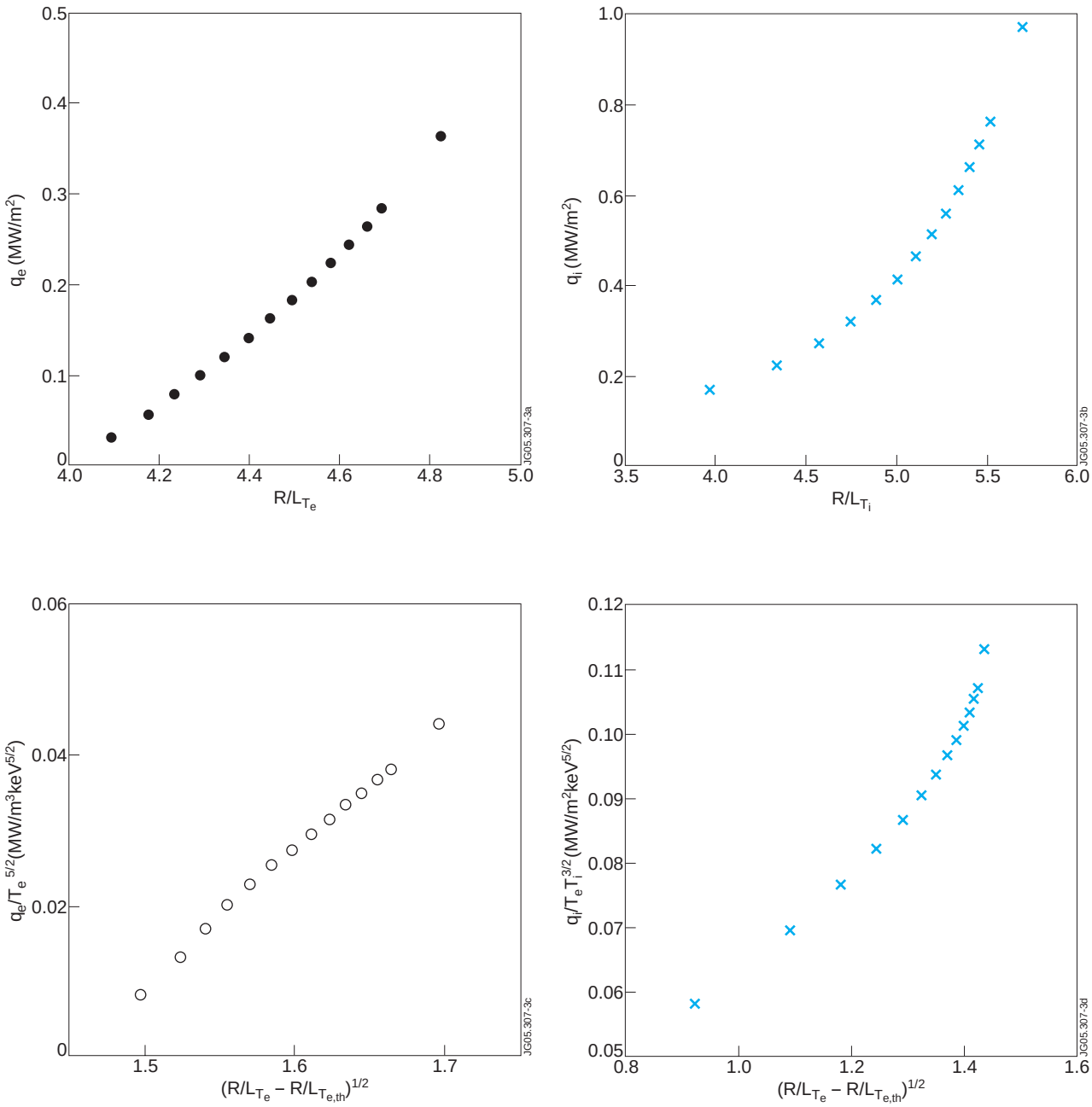

Figure 3. Heat flux responses and stiffnes for increasing ion heating.

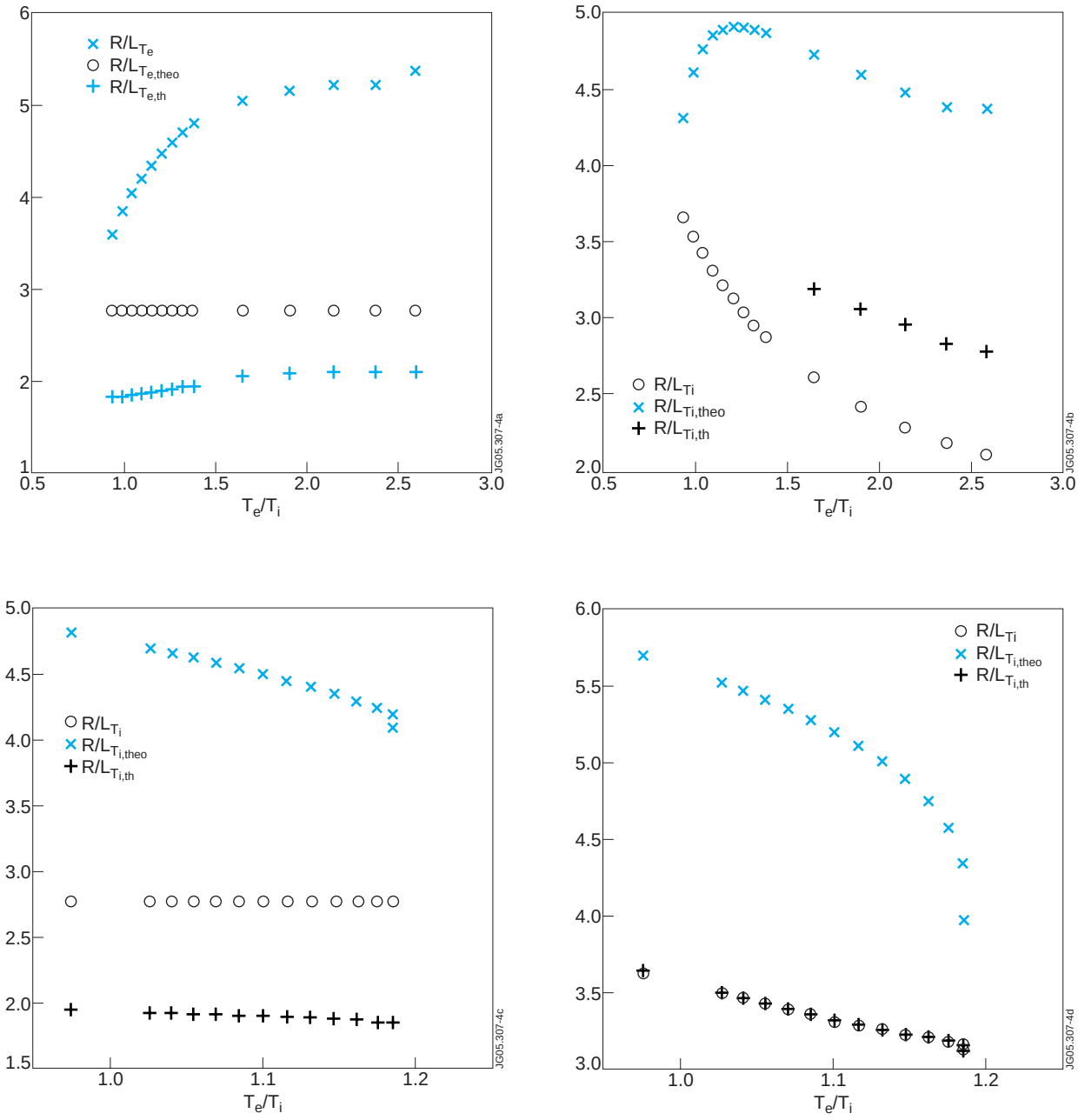

Figure 4. Thresholds vs T_e/T_i when the electrons are heated. R/L_T gives the temperature profile values, $R/L_{T,theo}$ is the analytical threshold from section 2 and $R/L_{T,th}$ are the thresholds calculated by the stand-alone code from Göteborg.

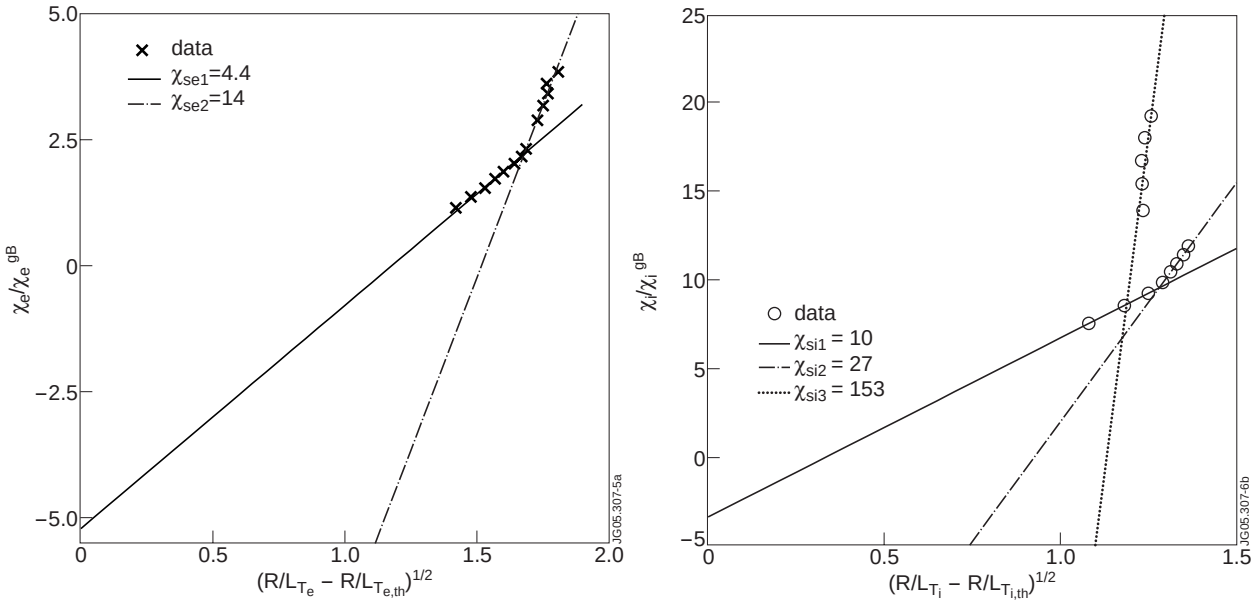

Figure 5. Calculation of χ_s for the electron heating case.

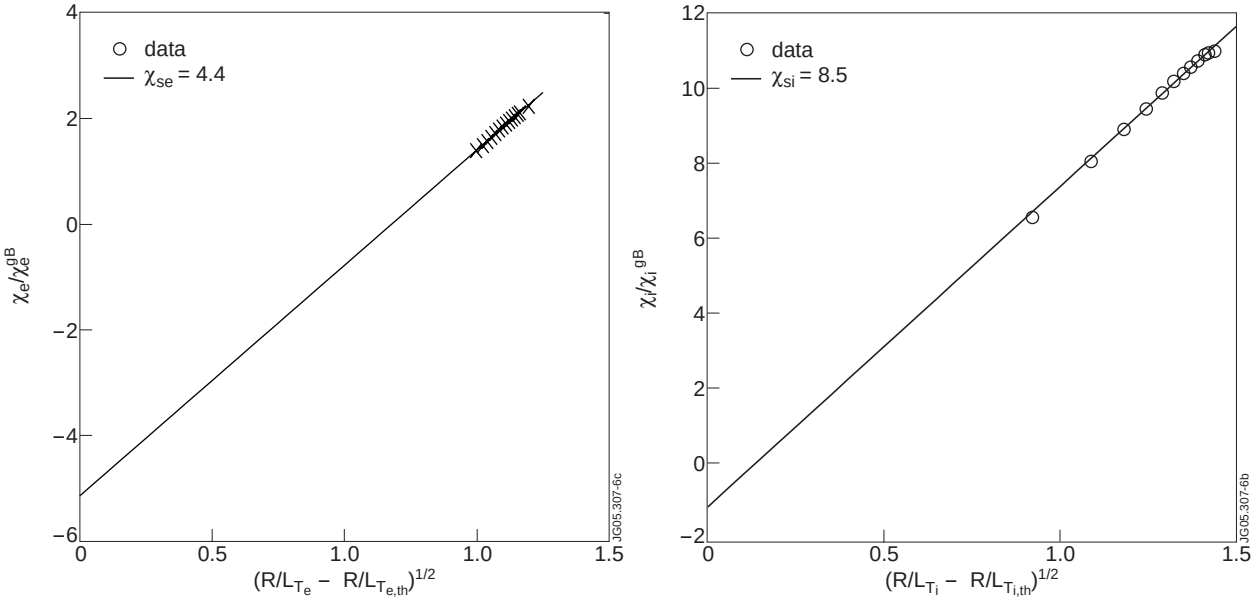

Figure 6. Calculation of χ_s for the ion heating case

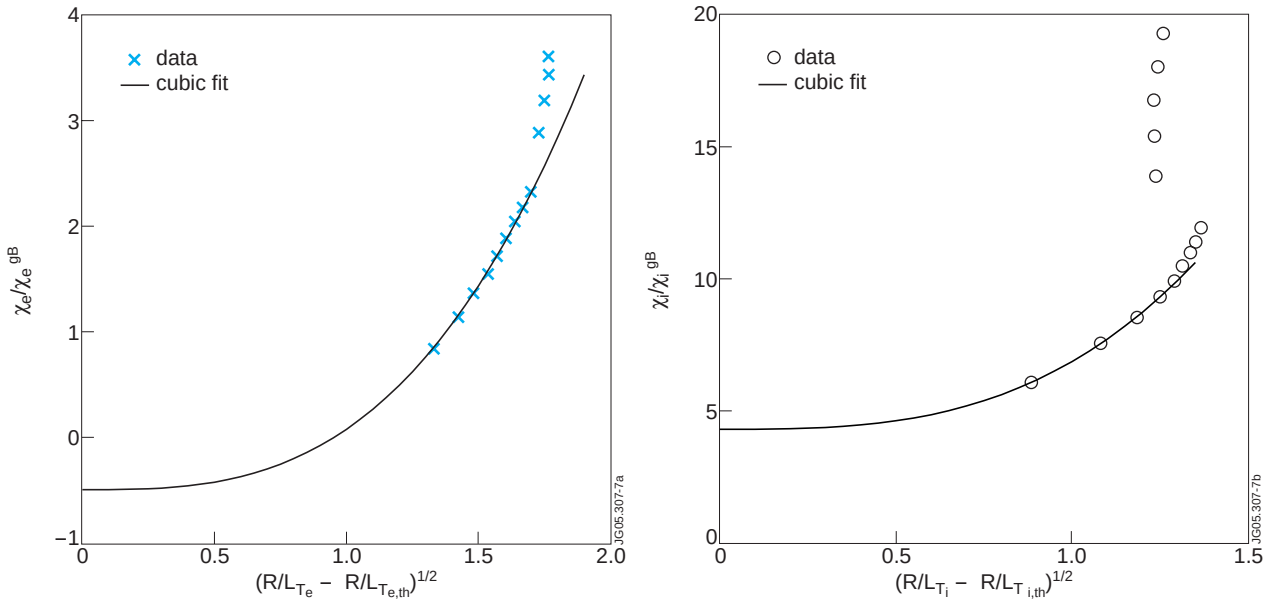

Figure 7. Cubic fit to χ_e and χ_i. The fitting parameter, $x= (R/L_T - R/L_{T,th})^{1/2}$.

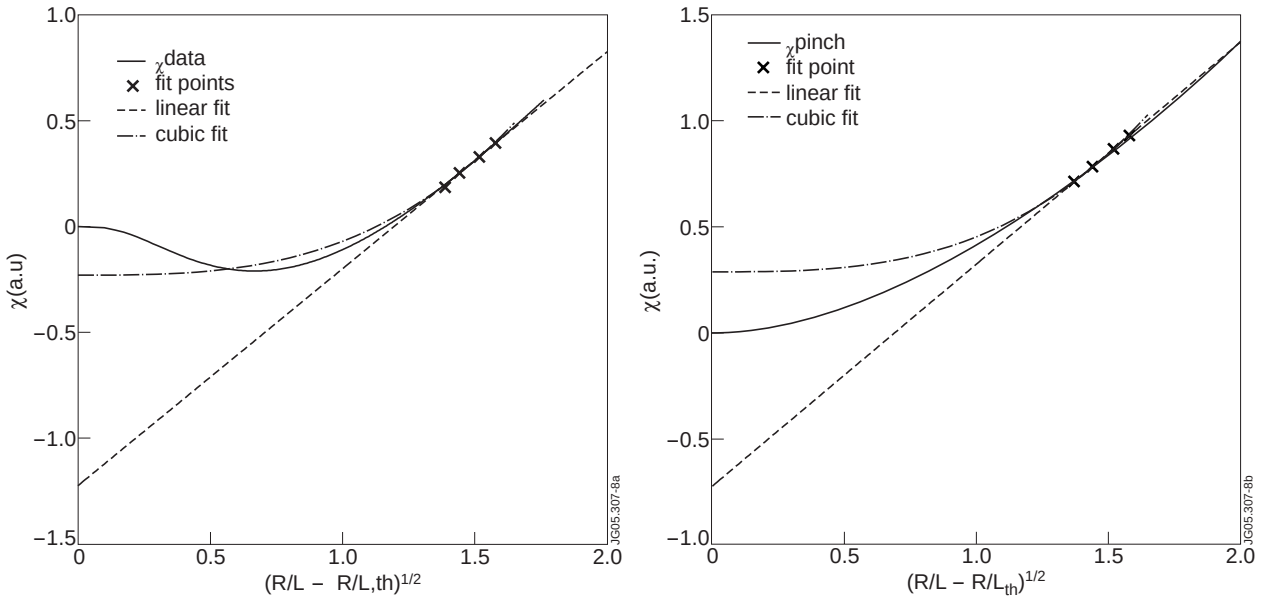

Figure 8. The effect of pinches on the heat diffusivity. The threshold, $R/L_T = 1.9$ in both (a) and (b).

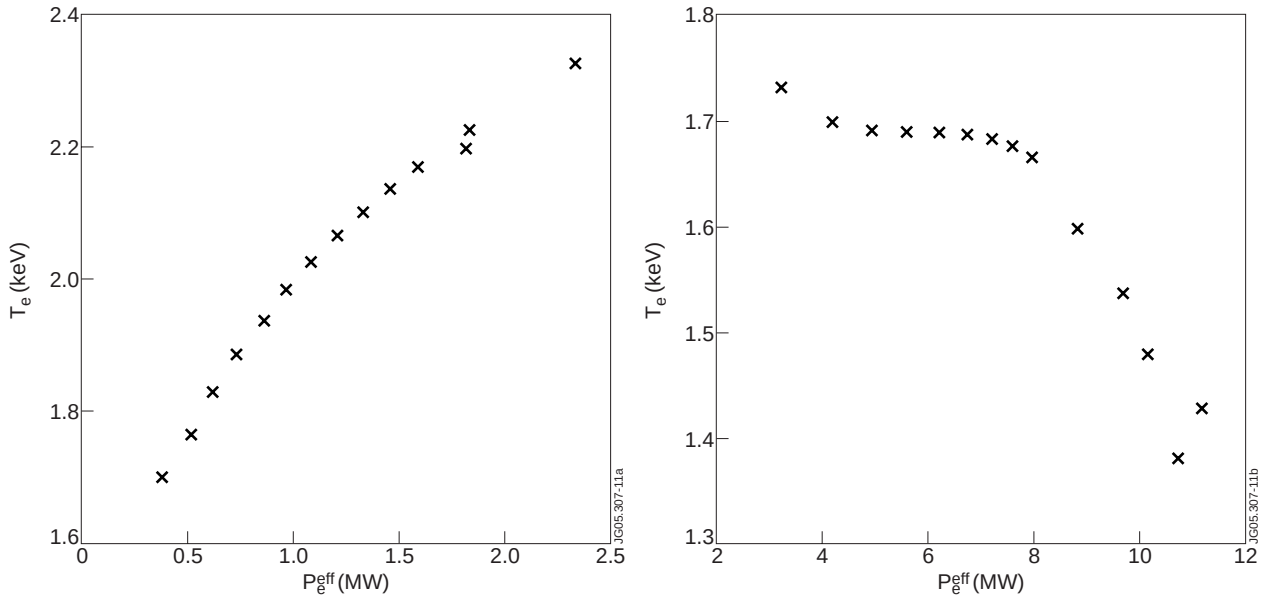

Figure A1. Effect of the increasing heating on the other species through thermal equilibration. The effective heating powers, $P_{e,i}^{eff}$, are evaluated at the same radial value as temperatures to increase the correlation between the plotted parameters.

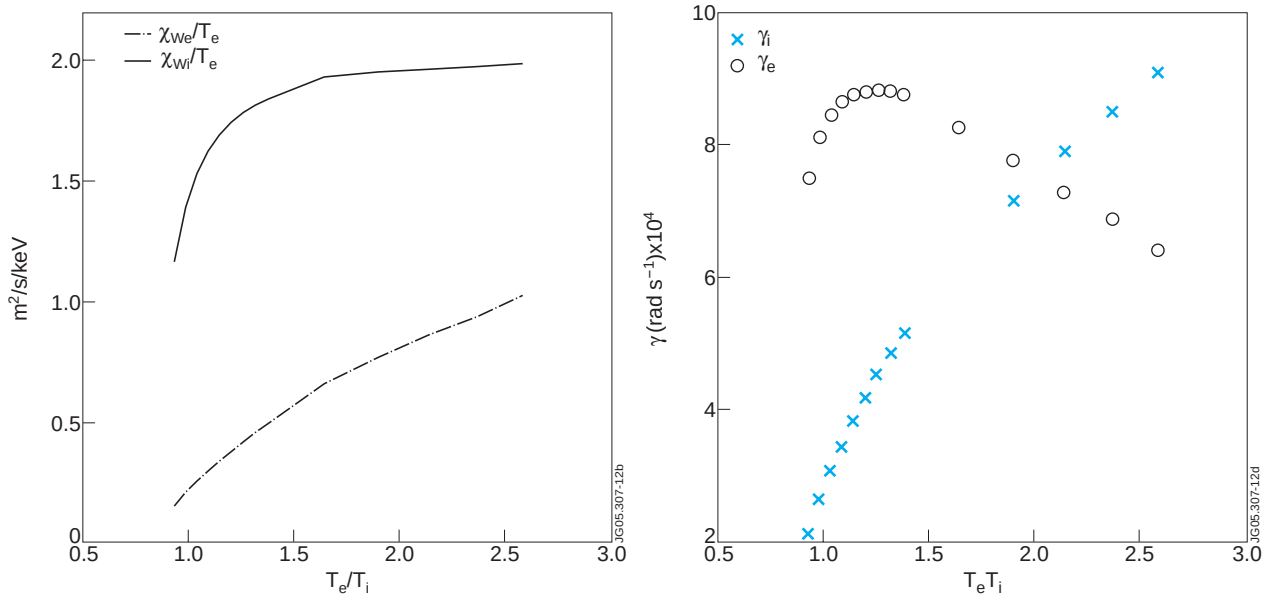

Figure B1. Comparison of diffusivities and growth rates to separate TE and ITG modes for increasing electron heating. The monotonically rising growth rate in (b) is concluded to be the TE mode, the parabolic-like the ITG mode. The ITG mode in the local-code is much smaller than in the JETTO ITG growthrates in (b). It is thus fair to conclude that the localcode overestimates the ITG thresholds in this region, which give rise to the discontinuity in $(R/L_{Ti} - R/LT_{i,th})^{1/2}$ seen in figure 2(d).

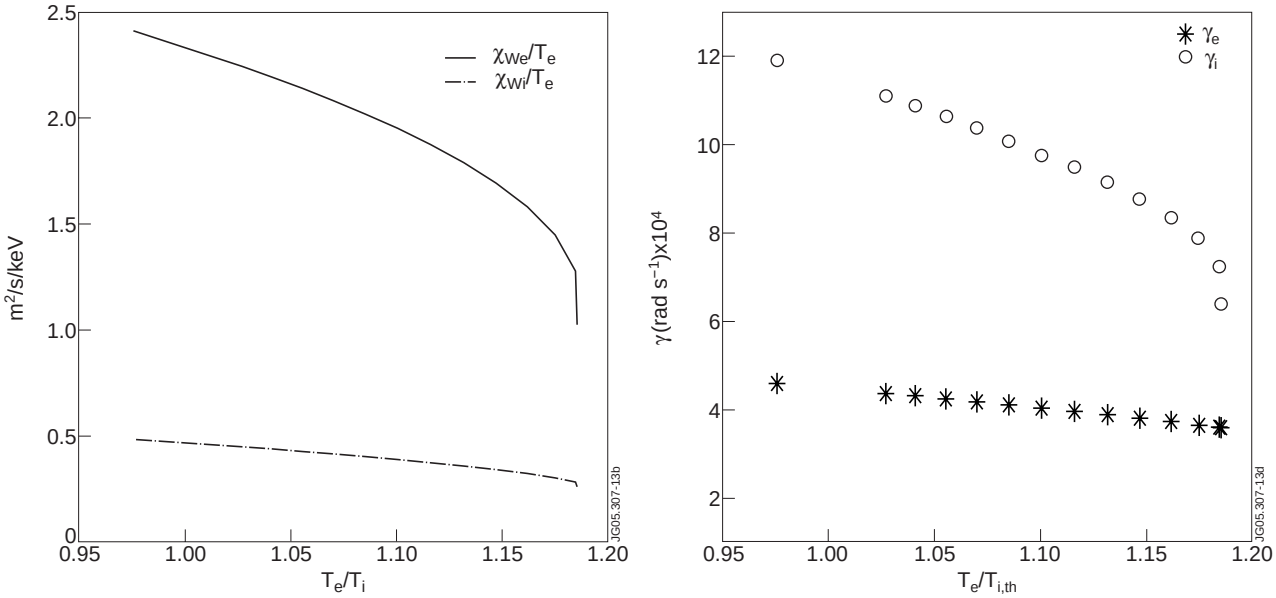

Figure B2. Comparison of diffusivities and growth rates to separate TE and ITG modes for increasing ion heating. The strongest instability in (b) is concluded to be the ITG mode, the smallest the TE mode.

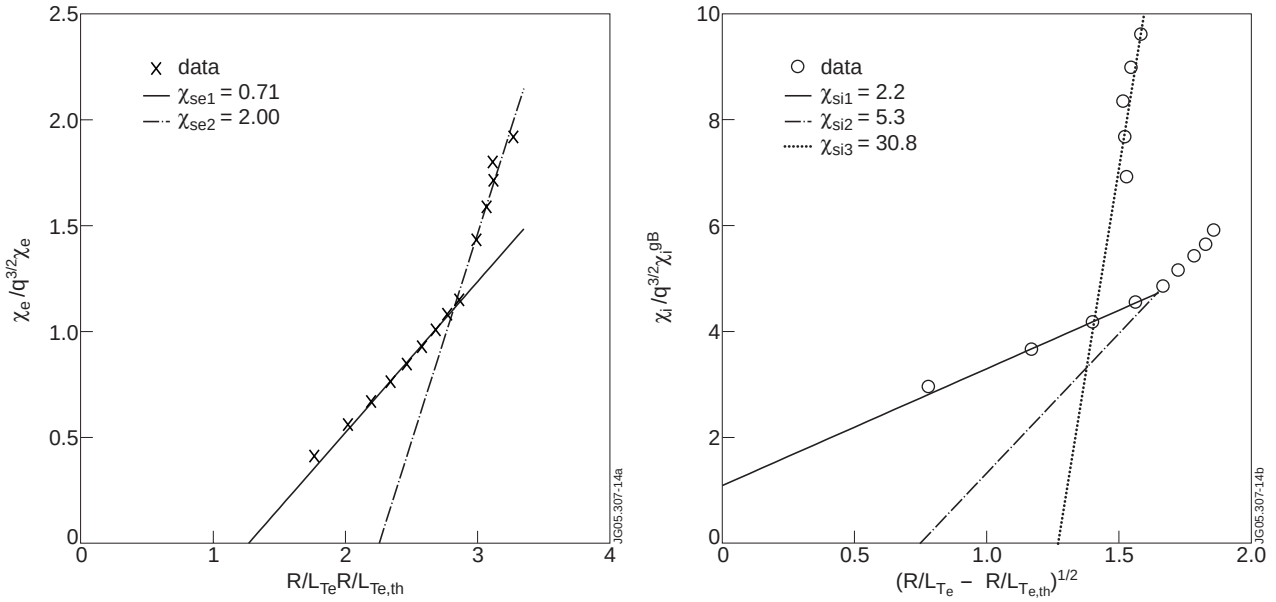

Figure C1. Calculation of empirical χ_s for the electron heating case.